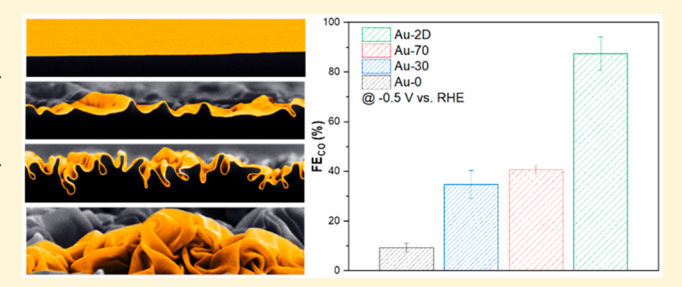
Downloaded via CORNELL UNIV on March 31, 2020 at 17:00:48 (UTC). See https://pubs.acs.org/sharingguidelines for options on how to legitimately share published articles.

Nano-folded Gold Catalysts for Electroreduction of Carbon Dioxide

Kam Sang Kwok, $^{\dagger,\bigcirc_{\bullet}}$ Yuxuan Wang, $^{\dagger,\bigcirc}$ Michael C. Cao, § Hao Shen, † Zimin He, † Gerald Poirier, $^{\bot}$ Brian E. McCandless, $^{\sharp}$ Kenneth J. Livi, $^{\dagger_{\bullet}}$ David A. Muller, $^{\S,\parallel_{\bullet}}$ Chao Wang, $^{*,\dagger_{\bullet}}$ and David H. Gracias*,†,‡

Supporting Information

ABSTRACT: The local structure and geometry of catalytic interfaces can influence the selectivity of chemical reactions. Selectivity is often critical for the practical realization of reactions such as the electroreduction of carbon dioxide (CO₂). Previously developed strategies to manipulate the structure and geometry of catalysts for electroreduction of CO₂ involve complex processes or fail to efficiently alter the selectivity. Here, using a prestrained polymer, we uniaxially and biaxially compress a 60 nm gold film to form a nanofolded electrocatalyst for CO2 reduction. We observe two



kinds of folds and can tune the ratio of loose to tight folds by varying the extent of prestrain in the polymer. We characterize the nano-folded catalysts using X-ray diffraction, scanning, and transmission electron microscopy. We observe grain reorientation and coarsening in the nano-folded gold catalysts. We measure an enhancement of Faradaic efficiency for carbon monoxide formation with the biaxially compressed nano-folded catalyst by a factor of about nine as compared to the flat catalyst (up to 87.4%). We rationalize this observation by noting that an increase of the local pH in the tight folds of the catalyst outweighs the effects of alterations in grain characteristics. Together, our studies demonstrate that nano-folded geometries can significantly alter grain characteristics, mass transport, and catalytic performance.

KEYWORDS: Catalysis, electrochemistry, nanomechanics, self-assembly, internal diffusion

E lectroreduction of carbon dioxide (CO₂) into valuable carbon-rich products is a potential solution to close the anthropogenic carbon cycle. 1,2 However, slow kinetics and low control over product yield and selectivity have hindered widespread commercial viability. 3,4 Nanostructured catalysts offer the potential to address these limitations.⁵ Indeed, a variety of nanoparticles, 6-9 thin films, 10-15 and nanoporous materials 16-21 have been explored, but there are still challenges with scalability, reproducibility, extreme reaction conditions, and cost. 6,10,12,16

Mechanical wrinkling of thin films using prestrained polystyrene (PS) substrates offers a facile, versatile, and costeffective strategy to create micro and nanostructured interfaces. This approach is compatible with nanoparticles, 22 nanoporous, ²³ thin films, ^{24,25} and two-dimensional (2D) materials (e.g., graphene and MoS_2), ^{26–31} and the morphology can be controlled using lithography. ^{27,28,32,33} Previous studies with wrinkled catalysts show improvement in some electrochemical reactions, including hydrogen evolution reaction (HER), 28,30,31,33 glucose sensing, 34,35 and DNA detection. 36 However, the previous studies involve only a single product reaction, and studies involving multiple reactions or those that measure selectivity are lacking.

Here, for the first time, we present evidence that a nanofolded gold (Au) catalyst can enhance the electroreduction of CO₂ reduction. We utilized a prestrained PS substrate to uniaxially or biaxially compress and create a novel Au catalyst with a combination of loose (>200 nm) and tight (<200 nm) folds (Figure 1). Importantly, we can control the ratio of tight to lose folds by varying the magnitude of the prestrain in the PS substrate. Also, we can release the nano-folded catalysts from the PS substrate and transfer them to alternate substrates or use them as freestanding catalysts. We characterized the nano-folded Au catalysts with scanning electron microscopy (SEM), X-ray diffraction (XRD), scanning transmission electron microscopy (STEM), and electron diffraction. XRD results suggest grain reorientation, and STEM studies show

Received: November 5, 2019 Published: November 18, 2019

[†]Department of Chemical & Biomolecular Engineering, Johns Hopkins University, Baltimore, Maryland 21218, United States

[‡]Department of Materials Science and Engineering, Johns Hopkins University, Baltimore, Maryland 21218, United States

[§]School of Applied and Engineering Physics, Cornell University, Ithaca, New York 14853, United States

Kavli Institute for Nanoscale Science, Cornell University, Ithaca, New York 14853, United States

¹Advanced Materials Characterization Lab, University of Delaware, Newark, Delaware 19716, United States

^{*}Institute of Energy Conversion, University of Delaware, Newark, Delaware 19716, United States

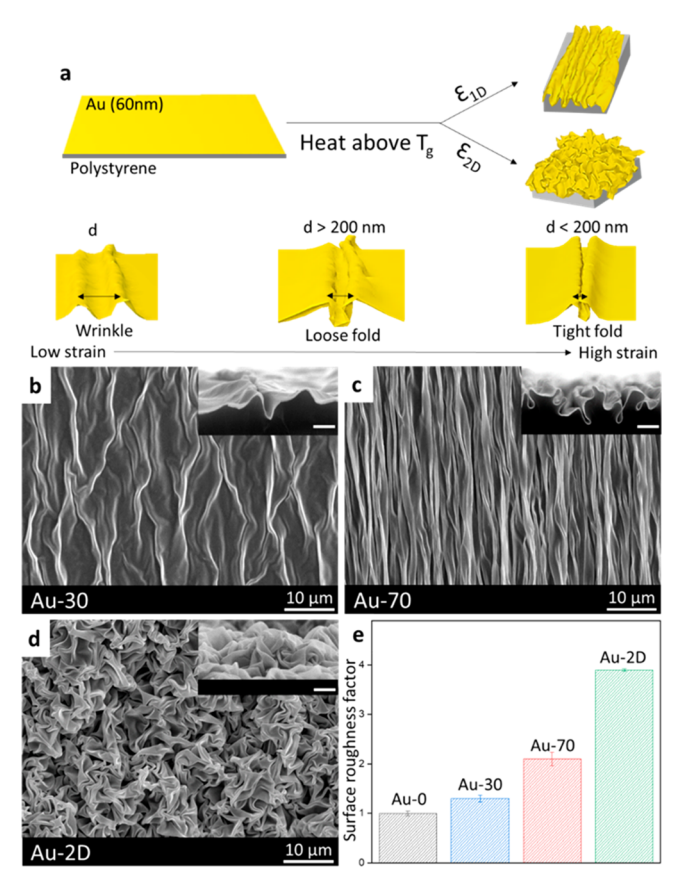


Figure 1. Schematic and fold characteristics of the Au catalysts. (a) Schematic illustrations of uniaxially or biaxially (2D) compressed Au catalysts formed using a prestrained PS substrate. Also shown are visual representations of a wrinkle, loose fold, and tight fold. (b–d) Top view and cross-sectional SEM images of (b) Au-30, (c) Au-70, and (d) Au-2D nano-folded Au catalysts. The inset shows zoomed images of the cross section of (b) Au-30, (c) Au-70, and (d) Au-2D. The inset scale bar represents 2 μ m. (e) Plot of the surface roughness factor of the Au catalysts as a function of uniaxial or biaxial strain.

grain coarsening in the nano-folded catalyst. Electrocatalytic studies indicate that the Faradaic efficiency (FE $_{\rm CO}$) of the nano-folded Au catalyst is approximately nine times higher than the flat Au catalyst. We attribute the enhanced selectivity to the nanofolds in the Au catalyst that generate high geometric current density, leading to an increase of the local pH, which suppresses the HER. 16,18,19

Our approach to preparing nano-folded Au catalysts is based on previous studies with some modifications (see Section 1.1 in the Supporting Information). Specifically, we thermally evaporated 60 nm of Au on prestrained PS at a rate of approximately 0.5 Å/s. After evaporation, we clamped and then heated the composite film above the glass transition temperature of PS to drive uniaxial and biaxial shrinkage with tunable macroscopic prestrain as measured by the ratio of the final to the initial length or area of the film (Figure 1a). Wrinkling of thin films using prestrained polymers has been attributed to minimizing the total energy of the system, including the membrane, bending and substrate energies, and wrinkling occurs when the prestrain is above a critical strain, $\varepsilon_{\rm cr} = \frac{1}{4} \left(\frac{3E_{\rm s}}{E_{\rm f}}\right)^{2/3}, \text{ where } \overline{E}_{\rm s} \text{ and } \overline{E}_{\rm f} \text{ are the plane-strain moduli}$ of the substrate and the thin film. Assuming representative

literature values for \overline{E}_f and \overline{E}_s , we estimate the critical strain to be 6×10^{-4} , which is significantly below our prestrain values.³⁷

In our studies, we investigated four prestrain conditions, which were 0% (Au-0, Figure S1), $\varepsilon_{1D} \sim 30\%$ (Au-30, Figure 1b), $\varepsilon_{1D} \sim 70\%$ (Au-70, Figure 1c), and area strain $\varepsilon_{2D} \sim 85\%$ (Au-2D, Figure 1d). Wrinkles formed at the lower values of prestrain can be further compressed into folds at higher values of prestrain.³³ We observed a greater fraction of loose (d > 200 nm) in Au-30 and a higher fraction of tight (d < 200 nm) folds at higher values of prestrain in Au-70. Specifically, we observed more than 40% of tight folds in Au-70 as compared to only about 3% of tight folds in Au-30 (Figure S2). Also, we estimated the surface roughness factor (RF) of the Au catalysts by dividing the electrochemical surface area (ECSA) to the geometric area of the nano-folded Au catalysts (Figure 1e and Figure S3). The surface roughness factors were 3.9 for Au-2D, 2.1 for Au-70, 1.3 for Au-30, and 1 for Au-0.

We characterized the microstructure of the flat and nanofolded Au catalysts by XRD and observed that, while the intensity of (200), (220), and (311) planes increased with increasing prestrain, the peaks did not shift or broaden (Figure 2a). These observations suggest that the changes in the nano-

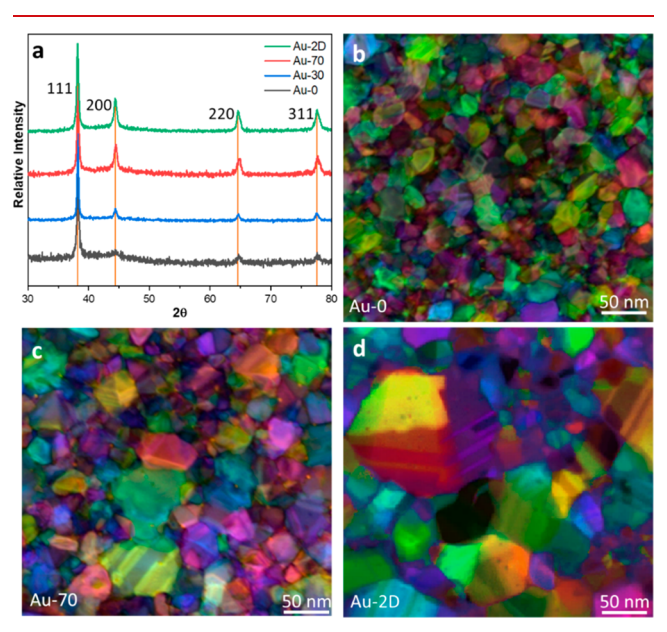


Figure 2. Characterization of the nano-folded catalysts using XRD and STEM. (a) XRD patterns of Au-0, Au-30, Au-70, and Au-2D. (b, c, d) 4D-STEM images of 30 nm thick Au-0, Au-70, and Au-2D.

folded samples are morphological; they introduce more diffraction planes and alter the grain structure with no significant changes in atomic displacement. We further characterized the surface of the nano-folded Au catalysts by grazing incidence XRD (GIXRD) and observed no significant strain after the compression. The deposited Au-0 film had a compressive strain of approximately 0.3%, which vanished after compression in all of the compressed samples (Figure S4).⁷ Previously, it has been reported that the grain structures of polycrystalline Au films can be altered dramatically when the deformation exceeds the elastic limit of Au,³⁹ and it is known that Au nanostructures undergo plastic deformation when the compressive strain is larger than 5%.⁴⁰ We attribute the increased XRD intensities of Au-30, Au-70, and Au 2D to preferred grain orientation, which was introduced by

compression. 41 We performed two control experiments to investigate if either the heating temperature or the orientation of the folds with respect to the X-ray beam affect the intensity of the XRD patterns (Figure S5), and we did not observe that neither factor had a measurable effect.

In order to investigate the microstructural changes in the nano-folded catalysts, we prepared and characterized thinned (30 nm) Au-0, Au-70, and Au-2D using 4D-STEM. 4D-STEM uses a pixelated detector to collect a diffraction pattern at every scanning point, creating a 4D data set. Analysis of the 4D diffraction data (see Supporting Information, S1.3) generates the false-colored grain images (Figure 2b-d). The STEM imaging and analysis were done in the convex regions of the folds, and we observed larger grains in the Au-2D (Figure 2d) as compared to Au-70 (Figure 2c) and Au-0 (Figure 2b), indicating grain coarsening in the nano-folded catalysts. This observation is consistent with previous studies on cyclic plastic deformation of Au thin films and indicates that the mechanical deformation can alter grain energetics and drive grain coarsening. 39,40,42,43 We further confirmed that grain coarsening does occur in 60 nm Au-70, which agrees with the observation of the 30 nm Au film (Figure S6). Also, the electron diffraction analysis indicates that the compression did not introduce new crystal planes in Au-2D and Au-70. The STEM diffraction patterns show a similar family of planes for Au-2D and Au-70, such as (111), (200), (220), and (311), as compared to Au-0, which also agrees with the XRD patterns (Figure S7).

An advantage of our approach is that the nano-folded catalysts are permanently deformed, and we can even release it from the PS substrate and transfer it to arbitrary substrates, such as flat silicon wafers and even curved syringe needles (Figure 3). Also, we can pick up the Au-70 with a tweezer without breakage, which suggests that compression strengthens the nano-folded catalysts (Figure 3e). Specifically, after the transfer, we observed that the average width of Au-30 and Au-70 decreased and increased by approximately 25% and 11%, respectively, while the height decreased by 29% and 8.7%, respectively (Table 1, Figures S9 and S10), and no deformation was induced in Au-0 (Figure S8). This observation can be rationalized by noting that the magnitude of the prestrain was high, and there is only a small extent of relaxation after release. For Au-30, we observed the collapse of the roof of the wrinkles, resulting in a decrease in both width and height, whereas, for Au-70, we observed relaxation by spreading the folds, resulting in an increase in width and a decrease in the height of the folds.

We investigated the electroreduction of CO₂ on these nanofolded Au catalysts using a home-built, gastight electrolysis cell. Details of the cell and electrocatalytic measurements are available in the Supporting Information (Figures S11 and S12). The total current density (per geometric area, J_{tot}) of Au-2D is significantly higher than the other Au catalysts, due to the higher surface roughness factors (Figure 4a). From the potential-dependent FE_{CO} plots (Figure 4b), Au-2D showed a higher efficiency of CO₂ reduction throughout the investigated potential region (from -0.5 V to -0.9 V versus the reversible hydrogen electrode, RHE; the same potential scale is used in the following discussion) and achieved a maximum FECO of 87.4% at -0.5 V, followed by 40.6%, 34.7%, and 9.2% for Au-70, Au-30, and Au-0, respectively, at this potential. The Au-2D also shows the highest partial current density for CO (I_{CO} , per geometric area; see Figure 4c), with 2.4 mA/cm^2 at -0.5 V,

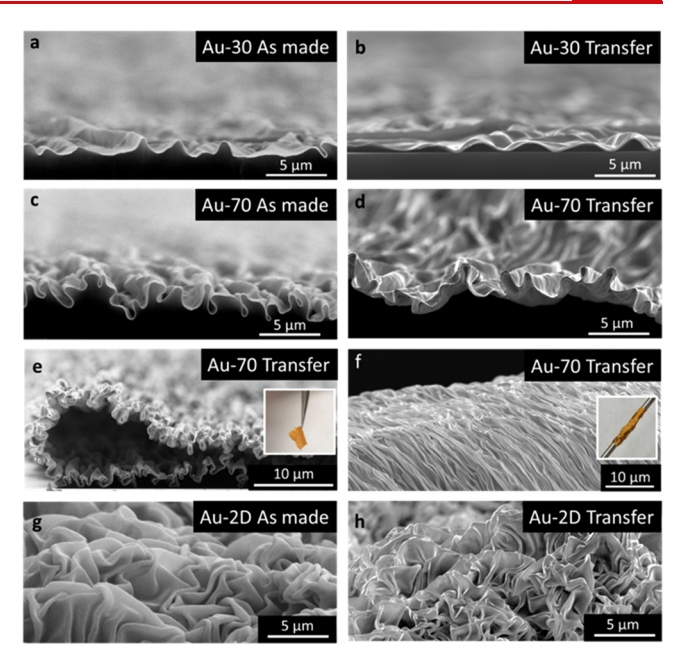


Figure 3. Characteristics of released and transferred nano-folded Au catalysts. (a–f) Cross-sectional SEM images of (a) Au-30 on the prestrained polymer, (b) Au-30 transferred from the prestrained polymer onto a silicon wafer, (c) Au-70 on the prestrained polymer, (d, e) Au-70 transferred from the prestrained polymer onto a silicon wafer, and (f) Au-70 transferred from the prestrained polymer onto a metal syringe needle. The insets in panels e and f are optical images. (g) Cross-sectional SEM images of Au-2D on the prestrain polymer, (h) Au-2D transferred from the prestrained polymer onto a silicon wafer.

Table 1. Properties of As-Made and Transferred Au Catalysts

| | no. of loose folds per line (folds/ | no. of tight folds per line (folds/ µm) | width (μm) | height (µm) | width difference after transfer (%) | height difference after transfer (%) |
|-----------|-------------------------------------|---|------------|-------------|---|--|
| Au- 30 | 0.15 | 0.005 | 2.60 | 0.72 | 25 | 29 |
| Au- 70 | 0.36 | 0.25 | 0.93 | 1.15 | 11 | 8.7 |

which represents an improvement factor of $\times 4$ over Au-70 (0.7 mA/cm²), $\times 4$ over Au-30 (0.6 mA/cm²) and $\times 16$ over Au-0 (0.15 mA/cm²).

The improvement in CO_2 reduction reaction activity and selectivity on Au surface is often attributed to surface structures effects, such as alloying, 44 undercoordinated facets, 45 and grain boundaries. However, the specific current density for CO normalized with the electrochemically active surface area (ECSA) (j_{CO} , Figure 4d) is consistent for the three types of nano-folded Au catalysts, which indicates a similar intrinsic activity for CO production. This finding suggests that the surface structure effect may not account for the observation of higher FE_{CO} and J_{CO} on the nano-folded Au of a larger roughness, albeit that it may contribute to the difference of J_{CO} between the pristine and nano-folded catalysts. On the other hand, the four Au electrocatalysts exhibit distinct HER activities during the CO_2 reduction, with Au-2D having the lowest ECSA-specific activity toward hydrogen (j_{H_2} , Figure 4e), followed by Au-70, Au-30, and Au-0. Therefore, the dramatic

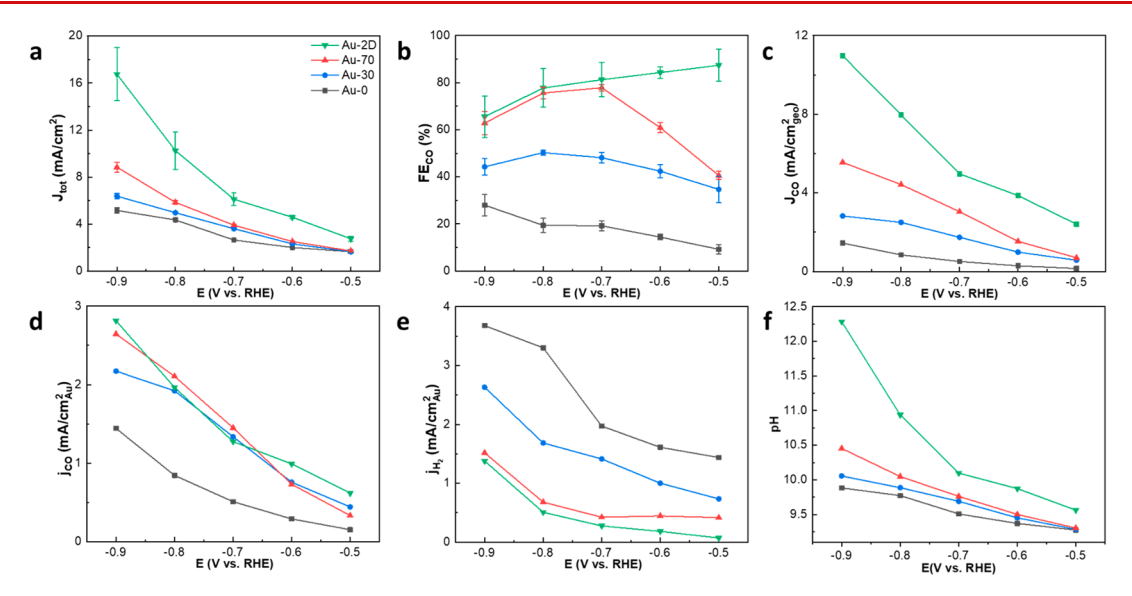


Figure 4. Electrocatalytic characteristics of the nano-folded Au catalysts. Plots of, (a) total current density per geometric area, (b) Faradaic efficiency, (c) CO current density per geometric area, (d) CO current density per ECSA, (e) H₂ current density per ECSA, and (f) simulated pH values. Au-0 (black), Au-30 (blue), Au-70 (red), and Au-2D (green).

difference in CO selectivity can be attributed to the suppressed HER on the nano-folded catalysts. This effect can be interpreted in terms of a rising local pH at high surface roughness. Multiple reports have shown suppression of HER with an increased pH, albeit with debatable mechanisms. 46 As shown in Figure 4f, we simulated the local pH conditions at the catalyst interfaces using the effective diffusivities of [CO₂]_{ao}, HCO₃⁻, CO₃²-, and OH⁻ and a previously reported mass transport model (see methods in Supporting Information). $^{52-54}$ At -0.5 V, we estimate the local pH to be 9.6 on the surface of Au-2D, the highest among the four nano-folded catalysts. The local pH rises at higher overpotentials, reaching the highest of 12.5 on Au-2D at -0.9 V, as compared to 11.4 on Au-70, 10.1 on Au-30, and 9.9 on Au-0. Au-2D was found to have the highest local pH throughout the potential range, corresponding to the most suppressed HER and highest FE_{CO} (Figure 4f).

In summary, we have demonstrated a new strategy to enhance the selectivity of CO formation by utilizing nanofolded Au catalysts for electroreduction of CO₂. To our knowledge, this is the first time that nano-folded catalysts have been applied to a reaction that involves multiple products and observed to significantly influence selectivity. Also, as compared to prior approaches to enhance selectivity, our catalysts achieve a similar high FE_{CO} (~87%), $^{10-14,16-21}$ yet can be made in a straightforward manner using a prestrained polymer substrate. The nano-folded catalysts can be transferred from the prestrained polymer to other substrates, which is important for the assembly of flexible electrochemical devices and sensors. $^{55-58}$

Our study utilizes a comprehensive set of microstructural studies involving X-ray and e-beam techniques. X-ray studies show morphological changes while STEM analysis indicates grain coarsening in nano-folded catalysts, which suggests a facile approach to modify grain morphology of the ultrathin (~30 nm) Au films. Finally, we reveal that tight fold morphologies can reduce mass transport of the electrolytic species, create a high local pH to reduce the activity of HER, and consequently, enhance CO selectivity. We find that the pH effects outweigh the effects of alterations in grain character-

istics. We anticipate that this strategy of creating folds in catalysts by strain engineering could be utilized as a convenient strategy to tune the selectivity of chemical reactions and also be generalized to other electrocatalysts.

ASSOCIATED CONTENT

S Supporting Information

The Supporting Information is available free of charge at https://pubs.acs.org/doi/10.1021/acs.nanolett.9b04564.

Details of the experiments and the simulations; characteristics of the nano-folded catalysts; X-ray diffraction and STEM studies of the Au catalysts; characteristics of the as-made and transferred nano-folded Au catalysts; electrochemical measurements of the Au catalysts; local pH modeling of the Au catalysts (PDF)

AUTHOR INFORMATION

Corresponding Authors

*E-mail: chaowang@jhu.edu. *E-mail: dgracias@jhu.edu.

ORCID ®

Kam Sang Kwok: 0000-0001-6000-7384 Kenneth J. Livi: 0000-0001-7728-5460 David A. Muller: 0000-0003-4129-0473 Chao Wang: 0000-0001-7398-2090 David H. Gracias: 0000-0003-2735-4725

Author Contributions

^OK.S.K. and Y.W. contributed equally.

Notes

The authors declare the following competing financial interest(s): Cornell University has licensed the EMPAD software to Thermo Scientific.

■ ACKNOWLEDGMENTS

This work was supported by the Air Force Office of Scientific Research MURI program (FA9550-16-1-0031) and the National Science Foundation (CMMI-1635443). Y.W., H.S.,

Z.H., and C.W acknowledge the support by the National Science Foundation (CBET-1803482). M.C.C. and D.A.M. acknowledge electron microscope facilities at Cornell University supported by the National Science Foundation (DMR-1719875 and DMR-1539918).

REFERENCES

- (1) Doman, L. EIA Projects 28% Increase in World Energy Use by 2040. www.eia.gov/todayinenergy/detail.php?id=32912 (accessed Jun 1, 2019).
- (2) Verma, S.; Lu, S.; Kenis, P. J. A. Nat. Energy 2019, 4 (6), 466–474.
- (3) Arán-Ais, R. M.; Gao, D.; Roldan Cuenya, B. Acc. Chem. Res. 2018, 51 (11), 2906-2917.
- (4) Wu, J.; Sharifi, T.; Gao, Y.; Zhang, T.; Ajayan, P. M. Adv. Mater. **2019**, 31 (13), 1804257.
- (5) Zhang, L.; Zhao, Z. J.; Gong, J. Angew. Chem., Int. Ed. 2017, 56 (38), 11326–11353.
- (6) Chen, Y.; Li, C. W.; Kanan, M. W. J. Am. Chem. Soc. 2012, 134 (49), 19969–19972.
- (7) Feng, X.; Jiang, K.; Fan, S.; Kanan, M. W. J. Am. Chem. Soc. **2015**, 137 (14), 4606-4609.
- (8) Lee, H. E.; Yang, K. D.; Yoon, S. M.; Ahn, H. Y.; Lee, Y. Y.; Chang, H.; Jeong, D. H.; Lee, Y. S.; Kim, M. Y.; Nam, K. T. ACS Nano 2015, 9 (8), 8384–8393.
- (9) Trindell, J. A.; Clausmeyer, J.; Crooks, R. M. J. Am. Chem. Soc. **2017**, 139 (45), 16161–16167.
- (10) Liu, M.; Pang, Y.; Zhang, B.; De Luna, P.; Voznyy, O.; Xu, J.; Zheng, X.; Dinh, C. T.; Fan, F.; Cao, C.; et al. *Nature* **2016**, *537* (7620), 382–386.
- (11) Saberi Safaei, T.; Mepham, A.; Zheng, X.; Pang, Y.; Dinh, C. T.; Liu, M.; Sinton, D.; Kelley, S. O.; Sargent, E. H. *Nano Lett.* **2016**, *16* (11), 7224–7228.
- (12) Mariano, R. G.; McKelvey, K.; White, H. S.; Kanan, M. W. Science **2017**, 358 (6367), 1187–1192.
- (13) Fang, Y.; Flake, J. C. J. Am. Chem. Soc. 2017, 139 (9), 3399-3405.
- (14) Li, J.; Chen, G.; Zhu, Y.; Liang, Z.; Pei, A.; Wu, C. L.; Wang, H.; Lee, H. R.; Liu, K.; Chu, S. *Nat. Catal.* **2018**, *1* (8), 592–600.
- (15) Wang, Y.; Raciti, D.; Wang, C. ACS Catal. 2018, 8 (7), 5657–5663.
- (16) Hall, A. S.; Yoon, Y.; Wuttig, A.; Surendranath, Y. J. Am. Chem. Soc. 2015, 137 (47), 14834–14837.
- (17) Zhang, W.; He, J.; Liu, S.; Niu, W.; Liu, P.; Zhao, Y.; Pang, F.; Xi, W.; Chen, M.; Zhang, W.; et al. *Nanoscale* **2018**, *10* (18), 8372–8376.
- (18) Welch, A. J.; DuChene, J. S.; Tagliabue, G.; Davoyan, A.; Cheng, W. H.; Atwater, H. A. ACS Appl. Energy Mater. 2019, 2 (1), 164–170.
- (19) Chen, C.; Zhang, B.; Zhong, J.; Cheng, Z. J. Mater. Chem. A 2017, 5 (41), 21955-21964.
- (20) Kim, J.; Song, J. T.; Ryoo, H.; Kim, J. G.; Chung, S. Y.; Oh, J. J. Mater. Chem. A **2018**, 6 (12), 5119–5128.
- (21) Hossain, M. N.; Liu, Z.; Wen, J.; Chen, A. Appl. Catal., B 2018, 236, 483–489.
- (22) Gabardo, C. M.; Yang, J.; Smith, N. J.; Adams-McGavin, R. C.; Soleymani, L. ACS Nano **2016**, 10 (9), 8829–8836.
- (23) Zhang, L.; Lang, X.; Hirata, A.; Chen, M. ACS Nano 2011, 5 (6), 4407–4413.
- (24) Fu, C. C.; Grimes, A.; Long, M.; Ferri, C. G. L.; Rich, B. D.; Ghosh, S.; Ghosh, S.; Lee, L. P.; Gopinathan, A.; Khine, M. *Adv. Mater.* **2009**, *21* (44), 4472–4476.
- (25) Gabardo, C. M.; Zhu, Y.; Soleymani, L.; Moran-Mirabal, J. M. Adv. Funct. Mater. **2013**, 23 (24), 3030–3039.
- (26) Leem, J.; Wang, M. C.; Kang, P.; Nam, S. Nano Lett. **2015**, 15 (11), 7684–7690.

(27) Lee, W. K.; Kang, J.; Chen, K. S.; Engel, C. J.; Jung, W. B.; Rhee, D.; Hersam, M. C.; Odom, T. W. *Nano Lett.* **2016**, *16* (11), 7121–7127.

- (28) Kim, J. Y.; Lim, J.; Jin, H. M.; Kim, B. H.; Jeong, S. J.; Choi, D. S.; Li, D. J.; Kim, S. O. *Adv. Mater.* **2016**, 28 (8), 1591–1596.
- (29) Choi, J.; Mun, J.; Wang, M. C.; Ashraf, A.; Kang, S. W.; Nam, S. *Nano Lett.* **2017**, *17* (3), 1756–1761.
- (30) Jung, W. B.; Cho, K. M.; Lee, W. K.; Odom, T. W.; Jung, H. T. ACS Appl. Mater. Interfaces 2018, 10 (1), 1347–1355.
- (31) Jung, W. B.; Yun, G. T.; Kim, Y.; Kim, M.; Jung, H. T. ACS Appl. Mater. Interfaces 2019, 11 (7), 7546-7552.
- (32) Yun, G. T.; Jung, W. Bin; Oh, M. S.; Jang, G. M.; Baek, J.; Kim, N. I.; Im, S. G.; Jung, H. T. Sci. Adv. 2018, 4 (8), No. eaat4978.
- (33) Huntington, M. D.; Engel, C. J.; Odom, T. W. Angew. Chem., Int. Ed. 2014, 53 (31), 8117-8121.
- (34) Adams-McGavin, R. C.; Chan, Y.; Gabardo, C. M.; Yang, J.; Skreta, M.; Fung, B. C.; Soleymani, L. *Electrochim. Acta* **2017**, 242, 1–9.
- (35) Chan, Y.; Skreta, M.; McPhee, H.; Saha, S.; Deus, R.; Soleymani, L. *Analyst* **2019**, *144* (1), 172–179.
- (36) Woo, S. M.; Gabardo, C. M.; Soleymani, L. Anal. Chem. 2014, 86 (24), 12341–12347.
- (37) Chapman, C. T.; Paci, J. T.; Lee, W. K.; Engel, C. J.; Odom, T. W.; Schatz, G. C. ACS Appl. Mater. Interfaces **2016**, 8 (37), 24339–24344.
- (38) Xue, Y.; Lee, W. K.; Yuan, J.; Odom, T. W.; Huang, Y. Langmuir 2018, 34 (51), 15749–15753.
- (39) Luo, X. M.; Zhu, X. F.; Zhang, G. P. Nat. Commun. 2014, 5 (1), 3021.
- (40) Wang, L.; Xin, T.; Kong, D.; Shu, X.; Chen, Y.; Zhou, H.; Teng, J.; Zhang, Z.; Zou, J.; Han, X. Scr. Mater. 2017, 134, 95–99.
- (41) Smallman, R. E.; Ngan, A. H. W. In *Modern Physical Metallurgy*; Elsevier, 2014; pp 415–442.
- (42) Glushko, O.; Cordill, M. J. Scr. Mater. 2017, 134, 95-99.
- (43) Glushko, O.; Dehm, G. Acta Mater. 2019, 169, 99-108.
- (44) Wang, Y.; Cao, L.; Libretto, N. J.; Li, X.; Li, C.; Wan, Y.; He, C.; Lee, J.; Gregg, J.; Zong, H.; et al. *J. Am. Chem. Soc.* **2019**, *141* (42), 16635–16642.
- (45) Zhu, W.; Michalsky, R.; Metin, Ö.; Lv, H.; Guo, S.; Wright, C. J.; Sun, X.; Peterson, A. A.; Sun, S. *J. Am. Chem. Soc.* **2013**, *135* (45), 16833–16836.
- (46) Strmcnik, D.; Uchimura, M.; Wang, C.; Subbaraman, R.; Danilovic, N.; Van Der Vliet, D.; Paulikas, A. P.; Stamenkovic, V. R.; Markovic, N. M. *Nat. Chem.* **2013**, *5* (4), 300–306.
- (47) Michalsky, R.; Zhang, Y. J.; Peterson, A. A. ACS Catal. 2014, 4 (5), 1274–1278.
- (48) Sheng, W.; Zhuang, Z.; Gao, M.; Zheng, J.; Chen, J. G.; Yan, Y. Nat. Commun. 2015, 6 (1), 5848.
- (49) Chen, X.; McCrum, I. T.; Schwarz, K. A.; Janik, M. J.; Koper, M. T. M. Angew. Chem., Int. Ed. 2017, 56 (47), 15025–15029.
- (50) Ledezma-Yanez, I.; Wallace, W. D. Z.; Sebastián-Pascual, P.; Climent, V.; Feliu, J. M.; Koper, M. T. M. Nat. Energy 2017, 2 (4), 17021
- (51) Cheng, T.; Wang, L.; Merinov, B. V.; Goddard, W. A. J. Am. Chem. Soc. 2018, 140 (25), 7787–7790.
- (52) Raciti, D.; Mao, M.; Park, J. H.; Wang, C. J. Electrochem. Soc. **2018**, 165 (10), F799-F804.
- (53) Raciti, D.; Mao, M.; Park, J. H.; Wang, C. Catal. Sci. Technol. 2018, 8 (9), 2364-2369.
- (54) Raciti, D.; Mao, M.; Wang, C. Nanotechnology 2018, 29 (4), 044001.
- (55) Pan, Y.-T.; Yin, X.; Kwok, K. S.; Yang, H. Nano Lett. 2014, 14 (10), 5953-5959.
- (56) Miyamoto, A.; Lee, S.; Cooray, N. F.; Lee, S.; Mori, M.; Matsuhisa, N.; Jin, H.; Yoda, L.; Yokota, T.; Itoh, A.; et al. *Nat. Nanotechnol.* **2017**, *12* (9), 907–913.
- (57) Zhu, B.; Gong, S.; Cheng, W. Chem. Soc. Rev. 2019, 48 (6), 1668–1711.

(58) Ray, T. R.; Choi, J.; Bandodkar, A. J.; Krishnan, S.; Gutruf, P.; Tian, L.; Ghaffari, R.; Rogers, J. A. *Chem. Rev.* **2019**, *119* (8), 5461–5533.